Pergamon

Int. J. Solids Structures Vol. 34, No. 12, pp. 1531–1546, 1997

0020–7683/97 $17.00 + .00

PII: S0020–7683(96)00083–2

STRESS PROPERTIES AT THE TIP OF A CONICAL NOTCH

Y. XU, L. M. KEER
Department of Civil Engineering, Northwestern University, Evanston, IL 60208, U.S.A.

and

V. K. LUK
Sandia National Laboratories, Albuquerque, NM 87185, U.S.A.

(*Received* 5 *September* 1994; *in revised form* 14 *May* 1996)

Abstract—The singular behavior of a three-dimensional conical notch under torsional or torsionless loading was analyzed using the Papkovich–Neuber displacement potential method. Based on the analysis of the Legendre polynomial with complex index λ_n (Thompson, T. R. and Little, R. W. (1970). End effects in a truncated semi-infinite cone, *Quart. J. Mech. Appl. Math.* **23**, 185–196), transcendental equations to the stress order λ_n of a torsional or torsionless notch at the cone tip are given for various notch angles. Analytical solutions for stress distributions around the cone tip under a concentrated torque T, and around the line notch tip under an expansion source E, are derived using the Legendre polynomial expression. These solutions can be applied for the study of penetration or perforation, where a penetrator is simulated as a concentrated force and as an expansion source. Curves of the first order eigenvalues show that there exist very weak singular stresses at the three-dimensional conical notch. According to the evidence observed in the conical notch experiment (Williams, M. L. (1966). Stress singular, adhesion, and fracture. In *Proc. 5th Nat. Congress for Appl. Mech.* pp. 451–464), when the base of a cone is loaded, fracture occurs along its side instead of at its tip. This observation suggests that there may exist a comparatively weak singularity at the cone tip.

1. INTRODUCTION

Stress analysis of a three-dimensional notch has wide engineering applications. For example, in penetration or perforation the stress distribution around the projectile tip dominates the penetrating behaviors, such as projectile resistance and target damage zone.

Studies of the singular behavior of a three-dimensional notch began with the work by Williams (1966) and later were addressed by Sih and Leibowitz (1968). It was experimentally observed that, by loading a ball bearing on the base of the cone as shown in Fig. 1, fracture did not take place at the cone tip but initiated along the side of the cone. Thompson and Little (1970), in their seminal studies of the end effects for a truncated cone, provided an effective analytical method, the Legendre polynomial analysis for the exterior problem, and

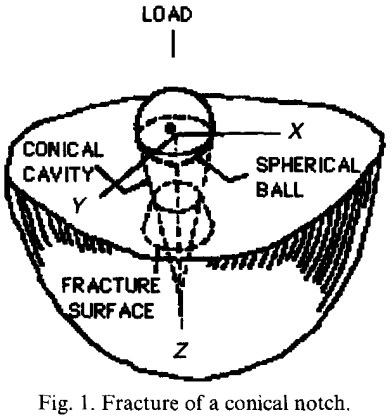

Fig. 1. Fracture of a conical notch.

derived the eigenequations for the solid cone problem. They considered only the case of the cone with an acute vertex angle. Later, Bazant and Keer (1974) directly applied these equations to analyze the singularity of the conical notch with general vertex angles. Somaratna and Ting (1986) derived the general eigenequations for three-dimensional conical notches in transversely isotropic materials.

The objective of this paper is to theoretically and systematically assess the singular order of stress at the cone tip and numerically calculate the leading terms of stress at the cone tip, when the cone is subjected to a torsional or torsionless loading. The complete expressions of displacements and stresses for the torsional or torsionless case are given using Legendre polynomial analysis. Special solutions of a conical notch under a concentrated force P and a concentrated torque T, as well as the solution of a line notch under an expansion source E are derived. These results are applied to the simulation of projectiles in penetration and perforation. Stresses induced by the concentrated force and torque have the singularities of R^{-2} and R^{-3}, respectively. This finding suggests that a torsional projectile may have better capabilities for penetration than the torsionless projectile.

2. BASIC FORMULATION

The Papkovich–Neuber displacement potential formulation is used to analyze the axisymmetrical cone in the spherical coordinate system (R, φ, θ). As shown in Fig. 2, the cone axis is defined along the z axis and the cone surface is at $\varphi = \varphi_0$. The cone is usually called a solid cone when $0 < \varphi_0 < \pi/2$ (Fig. 2) and a hollow cone when $\pi/2 < \varphi_0 < \pi$ (Fig. 3). The special case of a cone with $\varphi_0 = \pi$ is called a line notch.

The displacement field can be expressed in terms of Papkovich–Neuber functions in the form

$$2\mu\mathbf{u} = 4(1-\nu)\boldsymbol{\phi} - \nabla(\phi_0 + \mathbf{R}\cdot\boldsymbol{\phi}) \tag{1}$$

where $\mathbf{R} = (x, y, z)$ denotes the position vector, and μ and ν are the shear modulus and

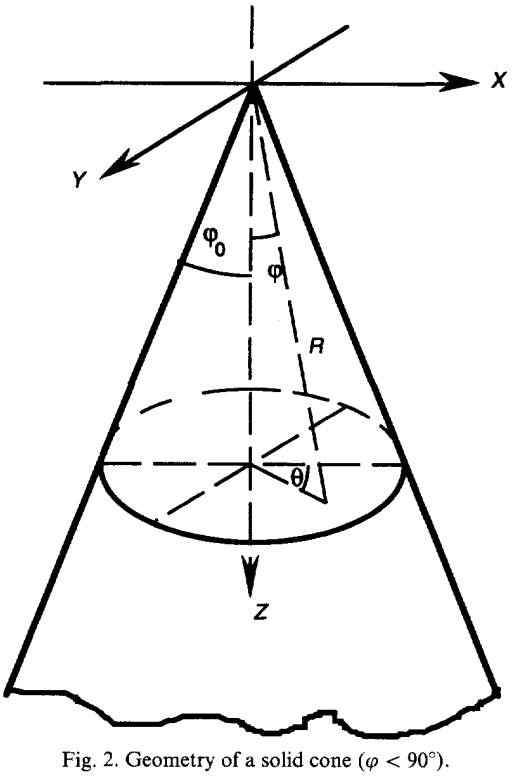

Fig. 2. Geometry of a solid cone ($\varphi < 90°$).

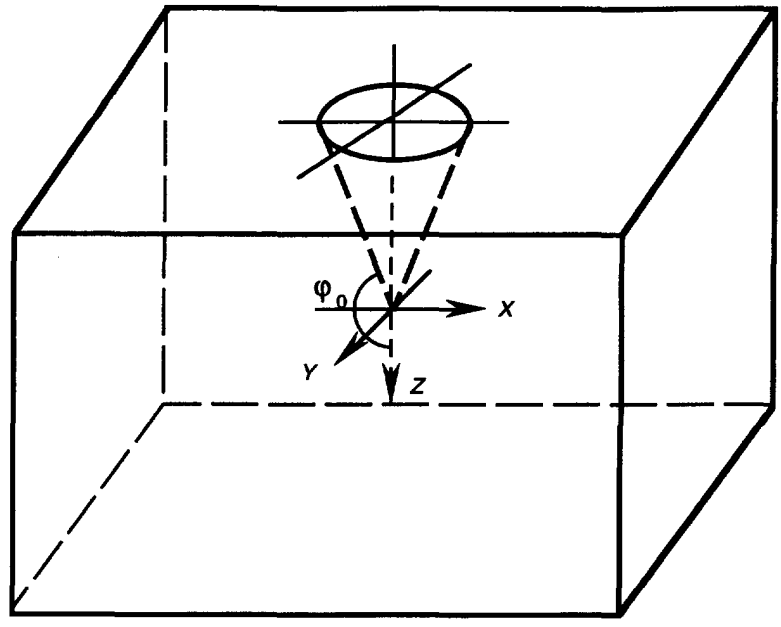

Fig. 3. Hollow cone in the solids ($\varphi_0 > 90°$).

Poisson's ratio, respectively. The scalar potential ϕ_0 and vector potential $\boldsymbol{\phi} = (\phi_1, \phi_2, \phi_3)$ in the Cartesian coordinate system satisfy the harmonic equations as

$$\nabla^2 \phi_j = 0, \quad (j = 0, 1, 2, 3). \tag{2}$$

In the spherical coordinate system, the displacements are noted as u_R, u_φ, and u_θ, which can, in terms of (1), be expressed as

$$\begin{aligned}
2\mu u_R(R, \varphi, \theta) &= 4(1-\nu)\phi_R - \frac{\partial}{\partial R}(\phi_0 + R\phi_R) \\
2\mu u_\varphi(R, \varphi, \theta) &= 4(1-\nu)\phi_\varphi - \frac{1}{R}\frac{\partial}{\partial \varphi}(\phi_0 + R\phi_R) \\
2\mu u_\theta(R, \varphi, \theta) &= 4(1-\nu)\phi_\theta - \frac{1}{R\sin\varphi}\frac{\partial}{\partial \theta}(\phi_0 + R\phi_R).
\end{aligned} \tag{3}$$

The transformation of the vector potential from the spherical coordinate system to the Cartesian coordinate system is

$$\begin{aligned}
\phi_1 &= \phi_R \sin\varphi\cos\theta + \phi_\varphi \cos\varphi\cos\theta - \phi_\theta \sin\theta \\
\phi_2 &= \phi_R \sin\varphi\sin\theta + \phi_\varphi \cos\varphi\sin\theta + \phi_\theta \cos\theta \\
\phi_3 &= \phi_R \cos\varphi - \phi_\varphi \sin\varphi.
\end{aligned} \tag{4}$$

The operator ∇^2 in the spherical coordinate system is

$$\nabla^2 = \frac{1}{R^2}\frac{\partial}{\partial R}\left(R^2\frac{\partial}{\partial R}\right) + \frac{1}{R^2\sin\varphi}\frac{\partial}{\partial \varphi}\left(\sin\varphi\frac{\partial}{\partial \varphi}\right) + \frac{1}{R^2\sin^2\varphi}\frac{\partial^2}{\partial \theta^2}. \tag{5}$$

For an axially symmetric problem, the harmonic function F can be written as

$$F = c_1 P_\lambda(z) + c_2 Q_\lambda(z)$$

where P_λ and Q_λ are the first and second kind of the Legendre function, respectively, with the real argument $z = \cos\varphi$. The degree λ of the Legendre functions is generally a complex number. For the three-dimensional conical notch, one must set $c_2 = 0$ to ensure that the solution is non-singular at $\varphi = 0$. Stresses of the axial symmetric problem in the spherical coordinate system can be expressed as

$$\sigma_{RR} = \left[(\lambda+2\mu)\frac{\partial}{\partial R} + 2\lambda\frac{1}{R}\right]u_R + \frac{1}{R}\left[\lambda\frac{\partial}{\partial\varphi} + \lambda\,\mathrm{ctan}(\varphi)\right]u_\varphi$$

$$\sigma_{\varphi\varphi} = \left[\lambda\frac{\partial}{\partial R} + 2(\lambda+\mu)\frac{1}{R}\right]u_R + \frac{1}{R}\left[(\lambda+2\mu)\frac{\partial}{\partial\varphi} + \lambda\,\mathrm{ctan}(\varphi)\right]u_\varphi$$

$$\sigma_{\theta\theta} = \left[\lambda\frac{\partial}{\partial R} + 2(\lambda+\mu)\frac{1}{R}\right]u_R + \frac{1}{R}\left[(\lambda\frac{\partial}{\partial\varphi} + (\lambda+2\mu)\,\mathrm{ctan}(\varphi)\right]u_\varphi$$

$$\sigma_{R\varphi} = \mu\frac{1}{R}\frac{\partial}{\partial R}u_R + \left(\frac{\partial}{\partial R} - \frac{1}{R}\right)u_\varphi,\ \sigma_{R\theta} = \mu\left(\frac{\partial}{\partial R} - \frac{1}{R}\right)u_\theta$$

$$\sigma_{\varphi\theta} = \mu\frac{1}{R}\left[\frac{\partial}{\partial\varphi} - \mathrm{ctan}(\varphi)\right]u_\theta. \tag{6}$$

In the torsionless case of $u_\theta = 0$, the shear stresses $\sigma_{R\theta}$ and $\sigma_{\varphi\theta}$ vanish. The boundary condition (i.e., the free tractions on the cone surface) results in $\sigma_{\varphi\varphi} = 0$, $\sigma_{R\varphi} = 0$ and $\sigma_{\varphi\theta} = 0$. This yields two kinds of problems. One is the exterior problem, where the displacements and stresses vanish at infinity. The other is the interior problem, where the displacement at the cone tip should be finite. The study of the asymptotic field at the cone tip is an interior problem.

3. LEGENDRE FUNCTION EXPRESSION OF A CONICAL NOTCH

The fundamental work on the three-dimensional solid cone under axisymmetric torsionless loading was successfully achieved by Thompson and Little (1970). They employed the Papkovich–Neuber displacement potential, using the Legendre function to derive the displacement and stress expressions, as well as eigenequation for the exterior problem of a solid conical notch, where no singularity exists. Using this method we attempt to systematically study the eigenequations for both exterior and interior problems under torsion or torsionless loading conditions for a conical notch. Furthermore, we propose that the weak singularity at the cone tip might explain the experimental phenomenon that fracture does not occur there. The completeness of the Legendre function expression has been discussed, and the general form of the displacement and stress expressions for the axially symmetric problem is given.

In the spherical coordinate system, the vector potential can be written as

$$\boldsymbol{\phi} = \phi_R\mathbf{e}_R + \phi_\varphi\mathbf{e}_\varphi + \phi_\theta\mathbf{e}_\theta \tag{7}$$

where ϕ_R, ϕ_θ and ϕ_θ, the components of the vector potential in the spherical coordinate system, in general, are not harmonic functions. The potential $\boldsymbol{\phi}$ in the Cartesian coordinate system is

$$\begin{aligned}\boldsymbol{\phi} = {} & (\phi_R\sin\varphi\cos\theta + \phi_\varphi\cos\varphi\cos\theta - \phi_\theta\sin\theta)\mathbf{e}_1 \\ & + (\phi_R\sin\varphi\sin\theta + \phi_\varphi\cos\varphi\sin\theta + \phi_\theta\cos\theta)\mathbf{e}_2 \\ & + (\phi_R\cos\varphi - \phi_\varphi\sin\varphi)\mathbf{e}_3.\end{aligned} \tag{8}$$

The harmonic equations (2) for $\boldsymbol{\phi}$ imply

$$\begin{aligned}\nabla^2(\phi_R\cos\varphi-\phi_\varphi\sin\varphi)&=0\\ \nabla^2[(\phi_R\sin\varphi+\phi_\varphi\cos\varphi+i\phi_\theta)\,e^{i\theta}]&=0\\ \nabla^2[(\phi_R\sin\varphi+\phi_\varphi\cos\varphi-i\phi_\theta)\,e^{-i\theta}]&=0\end{aligned}\tag{9}$$

which results in

$$\begin{aligned}\phi_R&=\sum_{n=-\infty}^{\infty}R^{\lambda_n}\{A_n(\cos^2\varphi-1)P'_{\lambda_n}(\cos\varphi)+C_n\cos\varphi P_{\lambda_n}(\cos\varphi)\}\\ \phi_\varphi&=\sum_{n=-\infty}^{\infty}R^{\lambda_n}\{A_n\cos\varphi P'_{\lambda_n}(\cos\varphi)+C_nP_{\lambda_n}(\cos\varphi)\}(-\sin\varphi)\\ \phi_\theta&=\sum_{n=-\infty}^{\infty}R^{\lambda_n}\{D_n\sin\varphi P'_{\lambda_n}(\cos\varphi)\}\\ \phi_0&=\sum_{n=-\infty\lambda_n\neq-1}^{\infty}R^{\lambda_n+1}B_nP_{\lambda_n+1}(\cos\varphi)+B_0^*\lg[R(1+\cos\varphi)].\end{aligned}\tag{10}$$

For the harmonic function ϕ_0, the term with eigenvalue equal to -1 does not make any contribution to the displacement (3). Instead of this term, the special term $B_0^*\lg[R(1+\cos\varphi)]$ might be added for the completeness of the displacement. The justification for adding the special term with B_0^* might be explained as the complete solution of displacement in u_R or u_φ may have the form

$$u=\sum_n c_nR^{\lambda_n}f_n(\varphi)\tag{11}$$

where f_n is an analytical function of φ. The Papkovich–Neuber displacement expression (3) requires that functions ϕ_R, ϕ_φ and ϕ_θ be in the form of (11). It can be seen from (3) that, for function ϕ_0 its differential terms $\partial\phi_0/\partial R$ and $(1/R)\,\partial\phi_0/\partial\varphi$ should also be in the form of (11). Therefore, function ϕ_0 has the form

$$\phi_0=d_n\frac{1}{\lambda_n+1}\sum_n R^{\lambda_n+1}g_n(\varphi)\tag{12}$$

which is similar to the form of (11). It is obvious that λ_n could not be -1 in (12) because ϕ_0 should be finite. For $\lambda_n=-1$ in (11), the corresponding term in (12) should have the form of $\phi_0^*=B_0^*\lg[RF(\varphi)]$. The non-singularity condition at $\varphi=0$ gives $\phi_0^*=B_0^*\lg[R(1+\cos\varphi)]$. The detailed proof for this is given in Appendix A. Therefore, displacements can be obtained by substitution of (10) into (3)

$$\begin{aligned}2\mu u_R&=\sum_{n=-\infty}^{\infty}R^{\lambda_n}\{E_n[4(1-\nu)-(\lambda_n+1)]\cos\varphi P_{\lambda_n}+F_n(\lambda_n+1)P_{\lambda_n+1}\}-\frac{1}{R}B_0^*\\ 2\mu u_\varphi&=\sum_{n=-\infty}^{\infty}R^{\lambda_n}\{-E_n[4(1-\nu)+\lambda_n]P_{\lambda_n}+(F_n-E_n)P'_{\lambda_n+1}\}\sin\varphi+\frac{1}{R}B_0^*\frac{\sin\varphi}{1+\cos\varphi}\\ 2\mu u_\theta&=\sum_{n=-\infty}^{\infty}R^{\lambda_n}4(1-\nu)\{-D_n\sin\varphi P'_{\lambda_n}\}\end{aligned}\tag{13}$$

where the coefficients $E_n=C_n-A_n(\lambda_n+1)$, $F_n=A_n[4(1-\nu)+(\lambda_n+1)]-B_n$, and P_{λ_n} are

Legendre functions with complex index λ_n. Substitution of (13) into (6) gives the stress expression as follows:

$$\sigma_{\varphi\varphi} = \sum_{n=-\infty}^{\infty} R^{\lambda_n-1}\{[\lambda_n^2+3\lambda_n+(3-2\nu)]\cos\varphi P_{\lambda_n} - 2(1-\nu)+(\lambda_n+1)P_{\lambda_n+1}$$
$$-\cos\varphi P'_{\lambda_n+1}\}a_n + \sum_{n=-\infty}^{\infty} R^{\lambda_n-1}\{-(1+\lambda_n)^2(3-2\nu)P_{\lambda_n+1}+\cos\varphi P'_{\lambda_n+1}\}b_n$$
$$-\frac{1}{k^2}B_0^*\frac{2\cos\varphi}{1+\cos\varphi}$$

$$\sigma_{R\varphi} = \sum_{n=-\infty}^{\infty} R^{\lambda_n-1}\{[2(1-\nu)-\lambda_n^2]\sin\varphi P_{\lambda_n} - [2(1-\nu)-\lambda_n]\sin\varphi P'_{\lambda_n+1}\}a_n$$
$$+\sum_{n=-\infty}^{\infty} R^{\lambda_n-1}\{-\lambda_n\sin\varphi P'_{\lambda_n+1}\}b_n - \frac{1}{R^2}B_0^*\frac{2\sin\varphi}{1+\cos\varphi}$$

$$\sigma_{RR} = \sum_{n=-\infty}^{\infty} R^{\lambda_n-1}\{-(\lambda_n^2-3\lambda_n+2\nu)\cos\varphi P_{\lambda_n} - 2\nu(\lambda_n+1)P_{\lambda_n+1}\}a_n$$
$$+\sum_{n=-\infty}^{\infty} R^{\lambda_n-1}\{\lambda_n(1+\lambda_n)P_{\lambda_n+1}\}b_n + \frac{1}{R^2}B_0^*$$

$$\sigma_{\theta\theta} = \sum_{n=-\infty}^{\infty} R^{\lambda_n-1}\{-(1-2\nu)(1+2\lambda_n)\cos\varphi P_{\lambda_n} - 2\nu(\lambda_n+1)P_{\lambda_n+1}+\cos\varphi P'_{\lambda_n+1}\}a_n$$
$$+\sum_{n=-\infty}^{\infty} R^{\lambda_n-1}\{(1+\lambda_n)P_{\lambda_n+1}-\cos\varphi P'_{\lambda_n+1}\}b_n - \frac{1}{R^2}B_0^*\frac{1}{1+\cos\varphi}$$

$$\sigma_{R\theta} = \sum_{n=-\infty}^{\infty} R^{\lambda_n-1}\{-(\lambda_n-1)\sin\varphi P'_{\lambda_n+1}\}d_n$$

$$\sigma_{\varphi\theta} = \sum_{n=-\infty}^{\infty} R^{\lambda_n-1}\{2\cos\varphi P'_{\lambda_n} - \lambda_n(\lambda_n+1)P_{\lambda_n}\}d_n \tag{14}$$

where $a_n = [1/4(1-\nu)]E_n$, $b_n = F_n$, and $d_n = 2(1-\nu)D_n$.

The eigenfunction can be derived using the traction free condition in terms of (14). It is clear that $\lambda_n = -1$ is one eigenvalue. The condition of free tractions on the cone surface, $\sigma_{\varphi\varphi}|_{\phi=\phi_0} = 0$ and $\sigma_{R\varphi}|_{\phi=\phi_0} = 0$, gives the other eigenequation for λ_n:

$$\det\begin{bmatrix} [\lambda_n^2+3\lambda_n+(3-2\nu)]\mu_0 P_{\lambda_n} & -(\lambda_n+1)^2 P_{\lambda_n+1}+\mu_0 P'_{\lambda_n+1} \\ +[(\lambda_n+1)^2+2(1-\nu)(\lambda_n+1)]P_{\lambda_n+1} & \\ [2(1-\nu)-\lambda_n^2]\sin\varphi P_{\lambda_n} - 2(1-\nu)\sin\varphi P'_{\lambda_n+1} & -\lambda_n\sin\varphi P'_{\lambda_n+1} \end{bmatrix} = 0 \tag{15}$$

where $\mu_0 = \cos\varphi_0$. This transcendental equation can be written as

$$(1+\lambda_n)^2\{\mu_0[(\mu_0^2-1)\lambda_n(1+\lambda_n)+2(1-\nu)\mu_0^2]P_{\lambda_n}^2(\mu_0)$$
$$-[(\mu_0^2-1)\lambda_n(2\mu_0^2\lambda_n+\mu_0^2+1)+4(1-\nu)\mu_0^2]P_{\lambda_n}(\mu_0)P_{\lambda_n+1}(\mu_0)$$
$$+\mu_0[(\mu_0^2-1)\lambda_n(1+\lambda_n)+2(1-\nu)]P_{\lambda_n+1}^2(\mu_0)\} = 0 \tag{16}$$

and the boundary condition $\sigma_{\varphi\theta}|_{\phi=\phi_0} = 0$ gives

$$(1+\lambda_n)\{[(2+\lambda_n)\mu_0^2-\lambda_n]P_{\lambda_n}(\mu_0)-2\mu_0 P_{\lambda_n+1}(\mu_0)\} = 0. \tag{17}$$

The eigenvalues are complex. Since the coefficients in (16) and (17) are real, the complex conjugate root is also a solution. Equations (16) and (17) represent the eigenvalues for torsionless and torsion problems, respectively. From further analysis it will be shown that any axially symmetric problem can be separated into a torsionless problem, which is determined by displacement components (u_R, u_φ), and a pure torsion problem, which is determined only by component u_θ.

4. CONCENTRATED TORQUE AT THE CONE TIP

The eigenvalues to (16) and (17) are not integers except for in the case of half space or line notch. For some special cases, $\lambda_n = -1$ is the solution of (16), and $\lambda_n = 0$ and $\lambda_n = -2$ are the solutions of (17). For a concentrated force and a concentrated torque at the cone tip, the stress solutions can be directly obtained from (14).

The concentrated force at the cone tip (Fig. 4a) can be given by taking $\lambda_n = -1$ for (14). The conditions of free traction on the conical notch surface, $\sigma_{\varphi\varphi}|_{\varphi=\varphi_0} = 0$ and $\sigma_{R\varphi}|_{\varphi=\varphi_0} = 0$, give

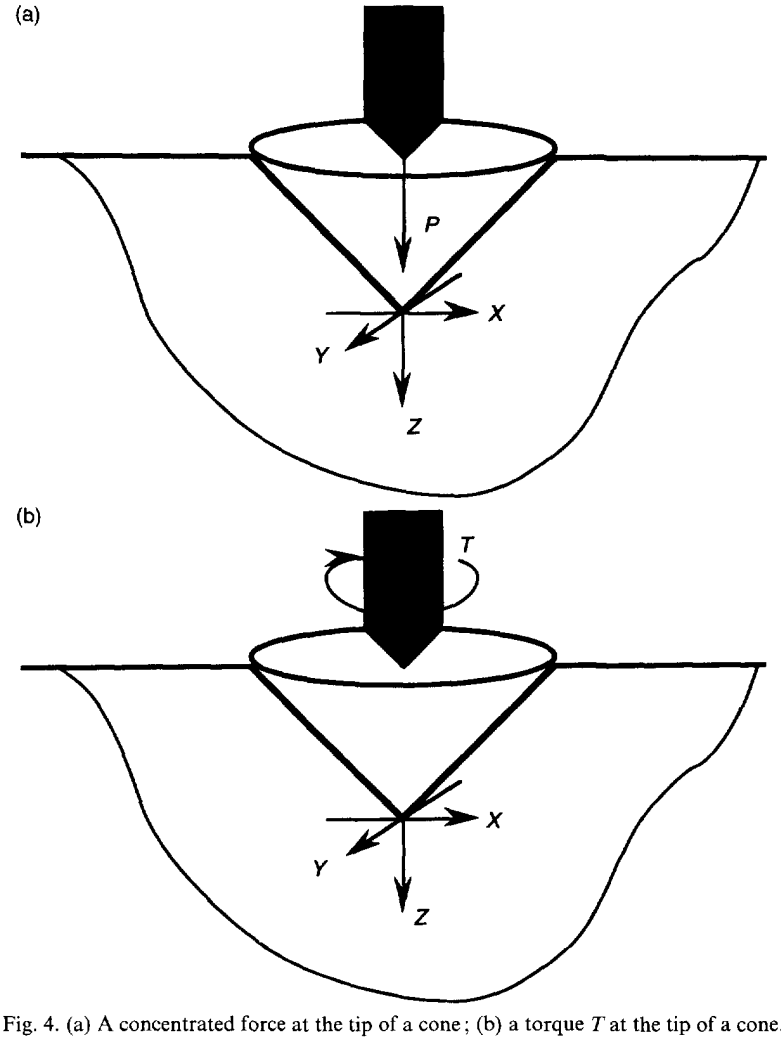

Fig. 4. (a) A concentrated force at the tip of a cone; (b) a torque T at the tip of a cone.

$$(1-2\nu)\cos\varphi a_{-1} - \frac{2\cos\varphi}{1+\cos\varphi}B^* = 0. \tag{18}$$

Substitution of (18) into (14) and the use of the equilibrium condition at the cone tip

$$P + 2\pi\int_0^{\varphi_0}(\sigma_{\varphi\varphi}\cos\varphi - \sigma_{R\varphi}\sin\varphi)R^2\sin\varphi\,\mathrm{d}\varphi = 0 \tag{19}$$

results in the stresses

$$\begin{aligned}
\sigma_{RR} &= \frac{P(1-2\nu)}{2\pi\alpha_0 R^2}\left\{1+\cos\varphi_0 - \frac{2(2-\nu)}{(1-2\nu)}\cos\varphi\right\}\\
\sigma_{R\varphi} &= \frac{P(1-2\nu)}{2\pi\alpha_0 R^2}\left\{\frac{\cos\varphi-\cos\varphi_0}{1+\cos\varphi}\sin\varphi\right\}\\
\sigma_{\varphi\varphi} &= \frac{P(1-2\nu)}{2\pi\alpha_0 R^2}\left\{\frac{\cos\varphi-\cos\varphi_0}{1+\cos\varphi}\cos\varphi\right\}\\
\sigma_{\theta\theta} &= \frac{P(1-2\nu)}{2\pi\alpha_0 R^2}\left\{\frac{\cos\varphi-\cos\varphi_0}{1+\cos\varphi} - 1 + \cos\varphi\right\}
\end{aligned} \tag{20}$$

and the displacements

$$\begin{aligned}
u_R &= \frac{P}{4\pi\mu\alpha_0 R}\{4(1-\nu)\cos\varphi - (1-2\nu)(1+\cos\varphi_0)\}\\
u_\varphi &= \frac{P}{4\pi\mu\alpha_0 R}\left\{(1-2\nu)\frac{(1+\cos\varphi_0)\sin\varphi}{1+\cos\varphi} - (3-4\nu)\sin\varphi\right\}
\end{aligned} \tag{21}$$

where the coefficient α_0 is

$$\alpha_0 = (1-\cos^3\varphi_0) - 2(1-\nu)\cos\varphi_0(1-\cos\varphi_0). \tag{22}$$

Solutions (20)–(22) are the same as those given by Little (1973), where the solution was derived by superposition of a Kelvin solution and the solution of center dilatation.

For the concentrated torque solution, $\lambda_n = -2$ is also an eigenvalue of equation (17), which makes possible the existence of the close form of the analytic solution for the conical notch under a concentrated torque. This solution combined with the concentrated force solution will play an important role in the application of stress analysis in drilling and penetration. The solution for a conical notch under concentrated torque can be derived as follows.

In terms of the analysis above, the axially symmetric displacement u_θ gives rise to the shear stress $\sigma_{R\theta}$ and $\sigma_{\varphi\theta}$. For the exterior pure torsion problem as shown in Fig. 4b, the displacement u_θ and stresses $\sigma_{R\theta}$ and $\sigma_{\varphi\theta}$ can be written as

$$2\mu u_\theta = \sum_{n=0}^{\infty} R^{\lambda_n}\{-2d_n\sin\varphi P'_{\lambda_n}\} \tag{23}$$

$$\begin{aligned}
\sigma_{\varphi\theta} &= \sum_{n=0}^{\infty} R^{\lambda_n-1}\{2\cos\varphi P'_{\lambda_n} - \lambda_n(\lambda_n+1)P_{\lambda_n}\}d_n\\
\sigma_{R\theta} &= \sum_{n=0}^{\infty} R^{\lambda_n-1}\{-\sin\varphi(\lambda_n-1)P'_{\lambda_n}\}d_n.
\end{aligned} \tag{24}$$

Consider the term $\lambda_n = -2$ for the concentrated torque problem, the displacement and shear stress

$$2\mu u_\theta = -\frac{1}{R^2} 2 \sin \varphi d_n, \tag{25}$$

$$\sigma_{R\theta} = \frac{1}{R^3} 3 \sin \varphi d_n, \quad \sigma_{\varphi\theta} = 0 \tag{26}$$

and the equilibrium equation

$$T + \int_0^{2\pi} \int_0^{\varphi_0} \sigma_{R\theta} R \sin \varphi R^2 \, d\varphi \, d\theta = 0 \tag{27}$$

results in

$$d_n = -\frac{T}{3\pi(\varphi_0 - \sin \varphi_0 \cos \varphi_0)}. \tag{28}$$

Thus, the displacement and stress induced by torque T are

$$2\mu u_\theta = \frac{2T}{3\pi(\varphi_0 - \sin \varphi_0 \cos \varphi_0)} \frac{\sin \varphi}{R^2}$$

$$\sigma_{R\theta} = -\frac{T}{\pi(\varphi_0 - \sin \varphi_0 \cos \varphi_0)} \frac{\sin \varphi}{R^3}. \tag{29}$$

The other components of displacement and stress vanish completely. The solution of the concentrated torque at the cone tip implies that: (1) the maximum displacement u_θ and shear stress $\sigma_{R\theta}$ occur either at the plane $\varphi = \pi/2$ for a hollow cone or at $\varphi = \varphi_0$ for a solid cone; (2) displacement u_θ decays with $1/R^2$ and shear stress decays with $1/R^3$; and (3) displacement on the surface depends on the factor $\sin \varphi_0/(\varphi_0 - \sin \varphi_0 \cos \varphi_0)$, which provides the maximum displacement when $\varphi_0 = \pi/2$. Figure 5 shows the surface displacement $u_\theta(\varphi_0) = (2T/3\pi R^2) f_u$ for various conical notch angles φ_0. As the cone angle increases, the displacement on the surface decreases.

The shear stresses induced by the torque and the concentrated force at the cone tip have the singularities $1/R^3$ and $1/R^2$, respectively. This result may offer an explanation for

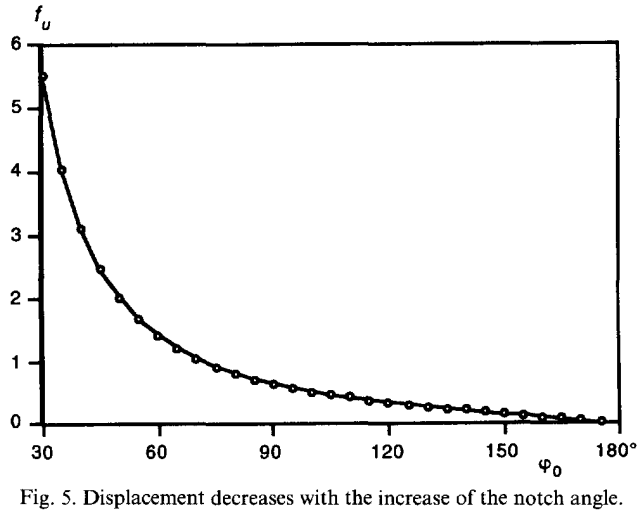

Fig. 5. Displacement decreases with the increase of the notch angle.

the fact that the torsional projectile has better capabilities for penetration than a torsionless projectile.

5. EXPANSION SOURCE IN LINE NOTCH AND SIMULATION OF PENETRATOR

The penetrating performance of a projectile can be investigated by studying the stress field generated in a target by a normal concentrated force and an expansion source. When a penetrator enters a target in some depth, the stress field generated by the normal concentrated force P for a line notch ($\varphi_0 = \pi$) in the range of $0 < \varphi < \pi$ takes the following form from (20):

$$\sigma_{RR} = -\frac{P}{2\pi\alpha_0 R^2}(1-2\nu)\frac{2(2-\nu)}{1-2\nu}\cos\varphi$$

$$\sigma_{R\varphi} = \frac{P}{2\pi\alpha_0 R^2}(1-2\nu)\sin\varphi$$

$$\sigma_{\varphi\varphi} = \frac{P}{2\pi\alpha_0 R^2}(1-2\nu)\cos\varphi$$

$$\sigma_{\theta\theta} = \frac{P}{2\pi\alpha_0 R^2}(1-2\nu)\cos\varphi \tag{30}$$

and the displacement can be written as

$$u_R = \frac{P}{8\pi(1-\nu)R}\{4(1-\nu)\cos\varphi\}.$$

$$u_\varphi = \frac{P}{8\pi(1-\nu)R}\{-(3-4\nu)\sin\varphi\}. \tag{31}$$

On the other hand, the projectile may generate another stress field that is induced by an expansion source, which can be evaluated by

$$E_z = \int_S T_r r\,\mathrm{d}s \tag{32}$$

where T_r is the traction in the r direction ($r = \sqrt{x^2+y^2}$). Thus, the circular expansion source can be written as

$$E_z = 2\pi\int_0^\pi (\sigma_{RR}\sin\varphi + \sigma_{R\varphi}\cos\varphi)R^3\sin^2\varphi\,\mathrm{d}\varphi. \tag{33}$$

The solution can be derived by taking $\alpha_n = -2$ in (14)

$$\sigma_{RR} = \frac{1}{R^3}\{[-2(5-\nu)\cos\varphi + 2\nu]c_n + 2d_n\}$$

$$\sigma_{R\varphi} = \frac{1}{R^3}\{-2(1+\nu)\sin\varphi\cos\varphi c_n\}$$

$$\sigma_{\varphi\varphi} = \frac{1}{R^3}\{[(1-2\nu)\cos^2\varphi + 2(1-\nu)]c_n - d_n\}. \tag{34}$$

This solution is self-equilibrated in the z direction. The traction-free notch surface gives

$$d_n = (3-4\nu)c_n. \tag{35}$$

Substitution of (35) into (34) yields

$$c_n = \frac{5E_z}{8\pi(6-5\nu)}. \tag{36}$$

Thus, the stress field generated by the expansion source is

$$\begin{aligned}
\sigma_{RR} &= \frac{5E_z}{8\pi(6-5\nu)R^3}[2(5-\nu)\cos^2\varphi - 6(1-\nu)] \\
\sigma_{R\varphi} &= \frac{5E_z}{8\pi(6-5\nu)R^3}[2(1+\nu)\sin\varphi\cos\varphi] \\
\sigma_{\varphi\varphi} &= \frac{5E_z}{8\pi(6-5\nu)R^3}[(1-2\nu)\sin^2\varphi] \\
\sigma_{\theta\theta} &= \frac{5E_z}{8\pi(6-5\nu)R^3}[3(1-2\nu)\sin^2\varphi].
\end{aligned} \tag{37}$$

The solution indicates that: (1) the stresses generated by an expansion source decay with the distance $1/R^3$; and (2) the circumferential stress in the θ direction is three times higher than that in the φ direction. This is why a star crack in penetration is likely to occur in the θ direction.

The target damage caused by a penetrator can be investigated by the combined effort of a concentrated force P associated with an expansion source E_z. The damage zone around the penetrator tip, induced by the normal force, is shown in Fig. 6a in terms of the Mises criterion. It can be seen that the maximum shear stress zone exhibits symmetry, but the stresses are opposite in regions ahead of and behind the cone tip. The damage zone induced by the expansion source is shown in Fig. 6b, where the stresses are symmetric for regions ahead of and behind the cone tip. For a projectile penetrating in a target, the combined damage zone affected by both the normal force and the expansion source is as shown in Fig. 6c, where the damage area ahead of the penetrator is larger than the damage area behind the penetrator. These predictive results are very close to some experimental findings.

6. EIGENVALUE CALCULATION AND SINGULAR ANALYSIS

In this section, the eigenvalue for various cones under torsion and torsionless loadings will be estimated with numerical methods. The results will show that: (1) the singularity of the conical notch is very weak when compared to the singularity of the two-dimensional crack problem, and (2) unlike crack propagation, where the tip stress singular order is a constant ($r^{-1/2}$), the conical notch tip extending a short distance is non-singular, because the line notch tip does have a non-singular stress distribution as that has been demonstrated by calculations. These are the reasons accounting for why the fracture does not occur at the tip of the conical notch.

The eigenvalues as determined by (16) were solved in two steps: (1) searching for stationary points in a given range, and (2) approaching the minimum absolute value of the left side (16), called modulus, in the local area.

In the first step, the whole area (the range of the roots to be searched) is divided by N to form a grid system with the distance between neighboring points equal to 0.1. For each point (x_j, y_j) in the grid system, the modulus is compared with neighboring points to find all the stationary points that satisfy $f(x_j, y_j) < f(x_j \pm h, y_j \pm h)$, $f(x_j, y_j) < f(x_j \pm h, y_j)$ and $f(x_j, y_j) < f(x_j, y_j \pm h)$, i.e., the point (x_j, y_j) has the minimum modulus among the 8 surrounding points. Here $f(x, y)$, the point modulus, represents the absolute value of the left side of (16). In the second step, for each stationary point $(x_j \pm h, y_j \pm h)$, the new area

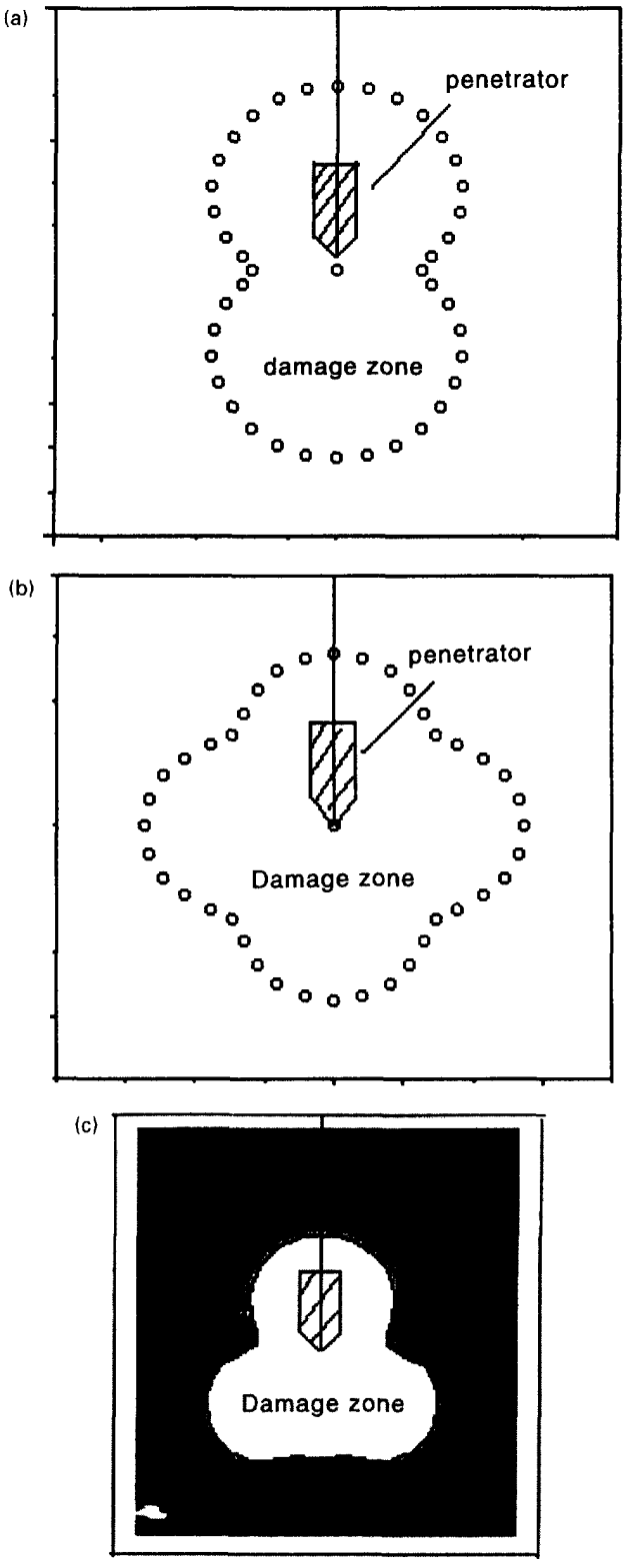

Fig. 6. (a) Damage zone around the penetrator induced by the normal force; (b) damage zone around the penetrator induced by the expansion source; (c) damage zone near the penetrator induced by the normal force and expansion source.

surrounding it can be divided by N_1 to form a new grid system. In each new grid system, the goal is to find the minimum modulus around the stationary point. This step can be repeated many times until the modulus is less than ε, the expected error.

Table 1. The first order eigenvalues for various cone angles ($\nu = 0.3$)

φ_0	15°	30°	45°	60	90°
$\mathrm{Re}(\lambda_1$	9.91737200	4.74087172	3.03712726	2.21186834	1.00000000
$\mathrm{Im}(\lambda_1)$	5.08497140	2.35890129	1.35202800	0.74249802	0.00000000
φ_0	105°	120°	135°	150°	165°
$\mathrm{Re}(\lambda_1)$	0.78740252	0.74563862	0.80118293	0.89782822	0.97486118
$\mathrm{Im}(\lambda_1)$	0.00000000	0.00000000	0.00000000	0.00000000	0.00000000

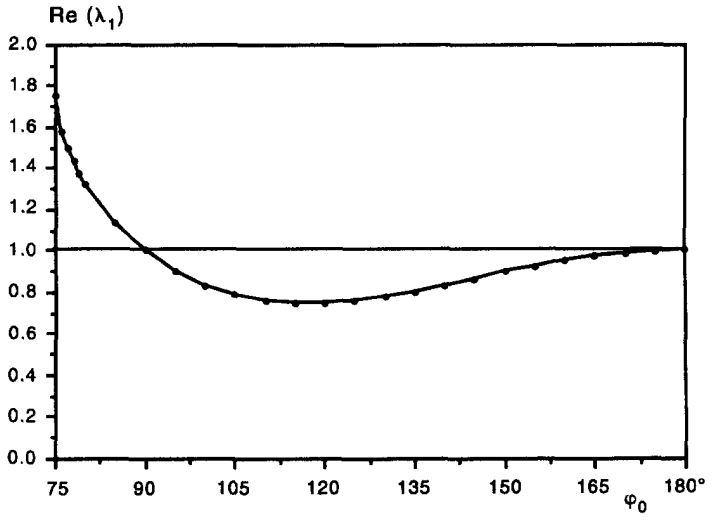

Fig. 7. Real part of λ_1 ($\nu = 0.3$) shows the weak singularity.

In the following example, the results yield 8 reliable digits with the expected error of 10^{-10}. The five leading eigenvalues for cone angles, 15°, 30° ... to 180° ($\nu = 0.25$) are listed in Appendix B. The first order eigenvalues for various cone angles with Poisson's ratio $\nu = 0.3$ are listed in Table 1. The real part of the eigenvalue is shown in Fig. 7. The eigenvalues for a conical notch with notch angle from 150° to 165° have eight reliable digits, and thus are exactly the same as those given by Klemm and Fernandes (1976) with the relation of $\lambda_n = b_{n-2}$.

The displacement at the cone tip is in the form of $R^{\lambda_n} f(\varphi)$ and the stress can be written as $R^{\lambda_n - 1} g(\varphi)$. The cone tip stress singularity is $R^{-\alpha_1}$ when $\mathrm{Re}(\lambda_1)$ is greater than zero and less than one, where $\alpha_1 = \mathrm{Re}(1 - \lambda_1)$. The greater α_1, the higher the singular stress. It can be concluded that:

(1) The real part of the first order eigenvalues is greater than one for the solid cone ($\varphi_0 < \pi/2$), and less than one for the hollow cone ($\varphi_0 > \pi/2$). For the special case of $\varphi_0 = \pi/2$ or π, the first order eigenvalues are one.

(2) The singular asymptotic field at the cone tip exists in the cone angle range from $\pi/2$ to π. For the special case of half space or line notch, there is a non-singular solution.

(3) The singular terms are weak as compared to the two-dimensional crack with a singular order of $r^{-1/2}$, and the higher singular term at the cone tip ($\nu = 0.3$) is about $R^{-0.25}$. The highest singular terms occur in the case of a cone angle around 120°. Then, α_1 decays quickly as the angle increases.

(4) When the cone angle is in the range of 150°–180°, the singular terms are very weak and the eigenvalue is almost 1.0.

Figure 8 shows the first eigenvalues of different cone angles for the materials with Poisson's ratio $\nu = 0.0, 0.25, 0.5$. The less the Poisson's ratio, the lower the singular stress. For example, when the cone angle is 165°, the singular order $\lambda_{n-1} = -0.06$.

For the pure torsional problem, the eigenequation (16) can be calculated as a torsionless problem. Figure 9 shows the first order eigenvalues of various notch angles under pure torsion loading. No singularity of stress exists at the cone tip since λ_1 is larger than one.

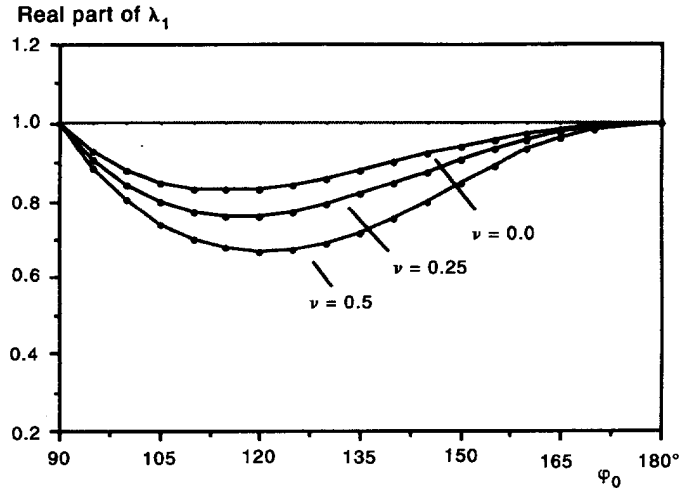

Fig. 8. The singularity of a conical notch as a function of Poisson's ratio ν.

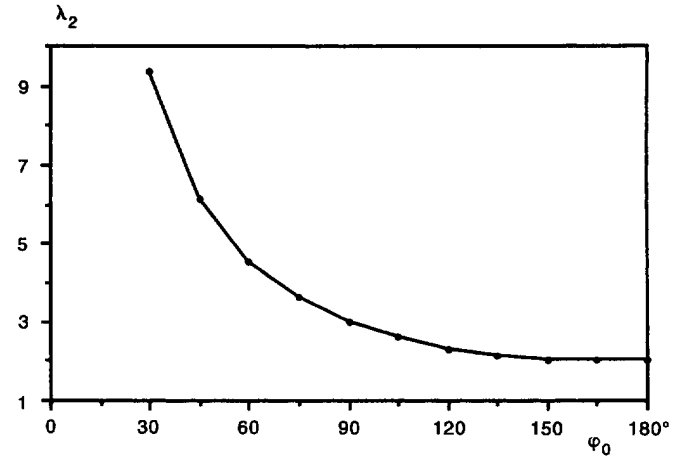

Fig. 9. The first order eigenvalues for a torsional notch.

7. CONCLUSION

The eigenequation for a conical notch analysis can be expressed as a transcendental equation with Legendre functions of the complex index. The singular stresses at the cone tip only occur in the hollow cone ($\pi/2 < \varphi_0 < \pi$). For the line notch ($\varphi_0 = \pi$), the eigenvalues are integers $(1, 2, 3, \ldots)$ and thus, no singular stress field exists at the cone tip.

The singularity of stress fields at the cone tip is weaker as compared to the two-dimensional crack. For the cone angle greater than 150°, the stress field around the cone tip is almost non-singular. On the other hand, if a conical notch tip advances a small distance, the tip will form a line notch, where the stresses are non-singular. Thus, the fracture toughness analysis could not be applied to the three-dimensional conical notch. The tip extension of a conical notch is a regular damage process, rather than a fracture process by the singular stresses. These stress properties of the conical notch may explain the experimental phenomenon that the damage zone occurs on the cone surface but not at the cone tip.

In projectile simulation, a penetrator can be simulated as a normal force associated with an expansion source at the cone tip. Stress analysis in the simulation shows that the damage area ahead of the penetrator is larger than the damage area behind the penetrator, which is in good agreement with the experimental measurements.

Acknowledgements—This work was supported by the United States Department of Energy under contract DE-AC04-94AL85000.

REFERENCES

Bazant, Z. P. and Keer, L. M. (1974) Singularity of elastic stresses and of harmonic functions at conical notches and inclusions. *International Journal of Solids and Structures* **10,** 957–964.

Klemm, J. L. and Fernandes, R. (1976) The three-dimensional hollow or solid truncated cone under axisymmetric torsionless end loading. *Journal of Applied Mechanics* **43,** 59–63.

Little, W. (1973) *Elasticity*, Prentice-Hall, Englewood Cliffs, NJ.

Sih, G. C. and Liebowitz, H. (1968) Mathematical theories of brittle fracture. In *Fracture*, Vol. II (ed. Liebowitz, H.), Academic Press, New York, pp. 67–190.

Somaratna, Nihal. and Ting, T. C. T. (1986) Three-dimensional stress singularities at conical notches and inclusions in transversely isotropic materials. *Journal of Applied Mechanics* **53,** 89–96.

Thompson, T. R. and Little, W. (1970) End effects in a truncated semi-infinite cone. *Quarterly Journal of Mechanics of Applied Mathematics* **23,** 185–196.

Williams, M. L. (1996) Stress singular, adhesion, and fracture. In *Proc. 5th U.S. National Congress of Appl. Mech.*, 14–17 June, Minneapolis, MN, pp. 451–464.

APPENDIX A

If the displacement is a function of ϕ_0 in the case of $\lambda_n = -1$, then the potential function ϕ_0 should satisfy

$$\frac{\partial \phi_0}{\partial R} = \frac{1}{R} f_1(\varphi), \quad \frac{1}{R}\frac{\partial \phi_0}{\partial \varphi} = \frac{1}{R} f_2(\varphi). \tag{A1,2}$$

The first equation implies $\phi_0 = f_1(\varphi)\lg(R) + f(\varphi)$, and the second equation results in

$$\lg(R)\frac{\mathrm{d}}{\mathrm{d}\varphi} f_1(\varphi) + \frac{\mathrm{d}}{\mathrm{d}\varphi} f(\varphi) = f_2(\varphi). \tag{A3}$$

Thus, function $f_1(\varphi)$ must be constant and the function ϕ_0 can be written in the form

$$\phi_0 = c\lg[RF(\varphi)]. \tag{A4}$$

The harmonic condition for function ϕ_0 yields the equation to $F(\varphi)$ as

$$\frac{1}{\sin\varphi}\frac{\partial}{\partial \varphi}\left(\sin\varphi \frac{F(\varphi)}{\partial \varphi}\right) = -1. \tag{A5}$$

The solution of (A5) is

$$F(\varphi) = \lg(\sin\varphi) + c_0\left[\lg\left(\cos\frac{\varphi}{2}\right) - \lg\left(\sin\frac{\varphi}{2}\right)\right]. \tag{A6}$$

Since function $F(\varphi)$ should be analytical at $\varphi = 0$, the constant c_0 must be 1 and, therefore, function $F(\varphi) = \lg(1+\cos\varphi)$ and function ϕ_0 is in the form

$$\phi_0 = c\lg[R(1+\cos\varphi)]. \tag{A7}$$

APPENDIX B

The roots to (15) for materials with Poisson's ratio $v = 0.25$ are listed as follows:

	$\varphi_0 = 30°$		$\varphi_0 = 45°$
n	λ_n	n	λ_n
1	(4.69683972, 2.36384635)	1	(3.01073051, 1.35119532)
2	(11.08719164, 2.93316793)	2	(7.25211911, 1.77694133)
3	(17.20841709, 3.30441986)	3	(11.32416769, 2.03091680)
4	(23.27137082, 3.57236673)	4	(15.36161970, 2.21182458)
5	(29.31064734, 3.78179976)	5	(19.38505326, 2.35252908)

	$\varphi_0 = 60°$		$\varphi_0 = 75°$
n	λ_n	n	λ_n
1	(2.19608677, 0.73739315)	1	(1.80313363, 0.01000000)
2	(5.34660080, 1.11292773)	2	(4.21866691, 0.56962892)
3	(8.39000608, 1.31086387)	3	(6.63977782, 0.74253152)
4	(11.41272409, 1.44915839)	4	(9.05114080, 0.85794103)
5	(14.42704860, 1.55592931)	5	(11.45848239, 0.94556082)

	$\varphi_0 = 90°$		$\varphi_0 = 120°$
n	λ_n	n	λ_n
1	(1.00000000, 0.00000000)	1	(0.76231843, 0.00000000)
2	(2.00000000, 0.00000000)	2	(1.78828818, 0.25581304)
3	(3.00000000, 0.00000000)	3	(3.26639785, 0.42521885)
4	(4.00000000, 0.00000000)	4	(4.75830964, 0.51633394)
5	(5.00000000, 0.00000000)	5	(6.25444205, 0.58058041)

	$\varphi_0 = 135°$		$\varphi_0 = 150°$
n	λ_n	n	λ_n
1	(0.81715621, 0.00000000)	1	(0.90706219, 0.00000000)
2	(1.60533184, 0.17840722)	2	(1.28740265, 0.00000000)
3	(2.89042571, 0.37169362)	3	(1.74502683, 0.00000000)
4	(4.20349725, 0.45948376)	4	(2.63515069, 0.00000000)
5	(5.52636466, 0.51882664)	5	(3.79183104, 0.45495339)